Relaxation of the electron energy distribution function in the afterglow of a N_2 microwave discharge including space-charge field effects

V. Guerra,[1] P. A. Sá,[2] J. Loureiro[1]

[1]*Centro de Física dos Plasmas, Instituto Superior Técnico, 1049-001 Lisboa, Portugal*

[2]*DEEC, Faculdade de Engenharia, Universidade do Porto, 4050-123 Porto, Portugal*

The relaxation of the electron energy distribution function (EEDF) in the post-discharge of an $\omega/(2\pi)$ $=2.45$ GHz microwave discharge in N_2 has been investigated by solving the time-dependent Boltzmann equation, including a term taking into account electron losses by diffusion under the presence of a space-charge field. It is shown that although the high-energy tail of the EEDF is rapidly depleted in times of 10^{-7} s ($p=2$ and 10 Torr), the electron density $n_e(t)$, the electron transport parameters, and the rate coefficients for some processes induced by electron impact, with energy thresholds typically smaller than ~2–3 eV, such as, e.g., stepwise excitation of $N_2(B\ ^3\Pi_g)$ and $N_2(C\ ^3\Pi_u)$ states from $N_2(A\ ^3\Sigma_u^+)$ metastables and excitation of $N_2(X\ ^1\Sigma_g^+,v)$ levels, are only slowly modified in the time interval $t\sim10^{-7}$–3×10^{-4} s due to the large characteristic times for ambipolar diffusion. As a result of modifications in $n_e(t)$, the change from ambipolar to free diffusion regimes occurs abruptly at $t\sim3\times10^{-4}$ and $\sim10^{-3}$ s for $p=2$ and 10 Torr, respectively.

I. INTRODUCTION

The study of N_2 post-discharges is currently receiving much attention, both experimental and theoretical, due to its great impact in applications related to surface treatments, such as steel surface nitriding [1–3] and plasma sources of N atoms [4,5]. Accordingly, spectroscopic studies of the most intense emission bands of N_2 (namely, the first and second positive systems of N_2) and N_2^+ (the first negative system, which in a post-discharge is usually called a *pink afterglow*) have been systematically investigated in several publications [4–6], with the aim toward a complete characterization of both the short-lived and remote afterglow regions. Moreover, the vibrational distribution of $N_2(X\ ^1\Sigma_g^+,v)$ molecules in the post-discharge [that is, the so-called vibrational distribution function (VDF)] was also studied by Raman-Stokes scattering [7], while the population of $N_2(A\ ^3\Sigma_u^+)$ metastables was measured in the afterglow of a flowing N_2 discharge by intracavity laser absorption spectroscopy [8], due to the strong coupling between both $N_2(X,v)$ and $N_2(A)$ species and the emissions from electronic states [9]. At the same time, we are unaware of any experiments to determine the electron energy distribution function (EEDF) in N_2 afterglow plasmas, with the exception of Ref. [10]. Finally, many features revealed in afterglow experiments were interpreted theoretically in Refs. [9, 11].

On the other hand, theoretical analyses have also been carried out, since the 1980s by Capitelli and co-workers, mainly on the coupling between the EEDF and the VDF of $N_2(X,v)$ molecules [12], as well as on the coupling between the EEDF and electronically excited states [13,14]. These studies have shown, among other aspects, that during the earlier and intermediate instants of the afterglow a very fast relaxation brings the EEDF to a quasistationary state with the VDF, in which the superelastic collisions of electrons with vibrationally excited molecules $N_2(X,v)$ compensate for the inelastic vibrational losses. The coupling between the EEDF and VDF was used in Ref. [15] to derive the vibrational

temperature of the VDF, by measuring the slope of the EEDF in the vibrational excitation region. In parallel, several studies have also been conducted on the variation of the electron density in decaying N_2 plasmas, using, for instance, a pulsed discharge [16] or a freely localized microwave discharge [17], and on the effect of electron-electron collisions on the EEDF in a decaying plasma [18].

However, in most studies on electron kinetics in a post-discharge, the relaxation of the EEDF was considered assuming that electron losses occur due to dissociative electron-ion recombination and free diffusion only, which leads to unrealistic fast relaxation times for the electron density, and for the electron transport parameters, due to the neglect of the transition from ambipolar to free diffusion regimes that occurs at the beginning of the afterglow [19–21]. In this paper, we report results of a theoretical study based on solutions to the time-dependent Boltzmann equation, written for a N_2 microwave post-discharge at $\omega/(2\pi)=2.45$ GHz in which a term for electron losses by diffusion in the presence of a space-charge field is considered. The transition from ambipolar to free diffusion regimes is assured by the monotonic reduction of the space-charge field, as the electron density decreases from the discharge to the post-discharge region, in a flowing afterglow. This approach allows us to obtain reliable data for the EEDF and related electron energy-averaged quantities that clearly constitute an improvement to previous works, and that are of great importance to interpret the afterglow experiments.

The present study shows that residual electron impact excitation maintains some efficacy in the post-discharge up to times of $\sim10^{-4}$ s, not only due to the vibrational superelastic heating of electrons but also as a consequence of the large characteristic time for electron losses by diffusion in the presence of a space-charge field. This effect is markedly visible for the case of stepwise electron excitation involving the impact of low-energy electrons, e.g., in excitation of $N_2(B\ ^3\Pi_g)$ and $N_2(C\ ^3\Pi_u)$ states from $N_2(A\ ^3\Sigma_u^+)$ metastables. The conclusions of the present paper are qualita-

tively in line with the spectroscopic observations realized in a N_2 rf pulsed post-discharge, where some evidence was found for the existence of electron impact excitation during the vibrational relaxation of $N_2(C,v')$ states [22]. The strong efficacy of the electron collision processes responsible for vibrational excitation are also shown to survive in a N_2 post-discharge up to $t \sim 1$ ms. In addition, the present results are in agreement with the variation of the effective diffusion coefficient, assuring the transition from ambipolar to free diffusion regimes, derived from breakdown time delay data [21]. Other aspects revealed in this work, such as the existence of the coupling between the EEDF and the VDF cited above, or the influence of electron-electron collisions on the EEDF, are globally in agreement with previous studies [12–15,18].

II. TIME-DEPENDENT ELECTRON BOLTZMANN EQUATION

In this section we will derive the final form taken by the time-dependent Boltzmann equation for electrons, as used in this paper, to study the relaxation of the EEDF in a N_2 afterglow. In such conditions, the Boltzmann equation needs to take into account the processes that produce a change on the electron density, such as the electron losses by electron-ion recombination and diffusion, the latter in the presence of a space-charge field. Moreover, the effects produced by the space-charge field should be progressively reduced from a discharge region to a post-discharge region, due to the monotonic decreasing of the electron density, since the first instants of the afterglow.

The standard procedure to study this problem starts with a Boltzmann equation usually written in the form [23,24]

$$\frac{\partial F}{\partial t} + \boldsymbol{\nabla}_{\mathbf{r}} \cdot (\mathbf{v}F) - \boldsymbol{\nabla}_{\mathbf{v}} \cdot \left(\frac{e\mathbf{E}}{m} F \right) = \left(\frac{\partial F}{\partial t} \right)_c, \tag{1}$$

where $F(\mathbf{r},\mathbf{v},t)$ is the electron velocity distribution function, constrained to the normalization condition $\int F \mathbf{dv} = n_e(\mathbf{r},t)$, with $\mathbf{dv}$ and n_e denoting a three-dimensional volume element in velocity space and the electron density, respectively; $\boldsymbol{\nabla}_{\mathbf{r}}$ and $\boldsymbol{\nabla}_{\mathbf{v}}$ are the gradient operators in configuration and velocity spaces, e and m are the electron absolute charge and mass, and the right-hand side member of Eq. (1) represents a collision operator taking into account the effects of two different types of elementary processes: (i) processes that keep the electron density constant, such as recoil collisions, inelastic, and superelastic collisions for excitation and deexcitation of rotational and vibrational levels of N_2, inelastic collisions for excitation of electronic states, and Coulomb collisions; and (ii) processes that produce a change on the electron number density, such as ionization and electron-ion recombination. Here we assume that the total electric field acting on the electrons consists of an applied HF field of frequency ω, and complex amplitude E_p, and a dc space-charge field E_s, as follows:

$$\mathbf{E}(\mathbf{r},t) = \mathbf{E_p} \exp(j\omega t) + \mathbf{E_g}(\lambda). \tag{2}$$

The amplitude $\mathbf{E_s}$ depends on position but $\mathbf{E_p}$ is assumed spatially constant.

Equation (1) may be solved by expanding F in spherical harmonics in velocity space and in Fourier series in time:

$$F = \sum_l \sum_k F_k^l P_l(\cos\theta) \exp(jk\omega t)$$

$$\simeq F_0^0 + \left(\frac{\mathbf{v}}{v} \right) \cdot [\mathbf{F_0^1} + \mathbf{F_1^1} \exp(j\omega t)]. \tag{3}$$

When the anisotropies resulting from the spatial gradients and the field are small, and for higher values of the field frequency ω, so that $\omega \gg \tau_e^{-1}$, with τ_e denoting the characteristic time for electron energy relaxation by collisions, all terms except the three indicated in Eq. (3) may be dropped. In a HF stationary discharge F_0^0, $\mathbf{F_0^1}$ and $\mathbf{F_1^1}$ are time-independent isotropic functions. The constancy of F_0^0 is associated with the so-called *effective field approximation* case, where the time variation of the alternating field is so rapid that the electrons only can see an average field [25]. The anisotropies are dictated by the action of the gradients of density and space-charge field, $\mathbf{F_0^1}$, and by the applied HF field, $\mathbf{F_1^1}$. In a HF discharge, constrained to the condition $\omega \gg \tau_e^{-1}$, we have $\partial F_0^0/\partial t = 0$, $\partial \mathbf{F_0^1}/\partial t = 0$ and $\partial \mathbf{F_1^1}/\partial t = j\omega \mathbf{F_1^1}$, with $j = \sqrt{-1}$. However, in order to extend this theory to a post-discharge, a time variation should be contemplated here in these three functions.

Inserting Eqs. (2) and (3) into Eq. (1) and then equating terms of similar angle dependence and periodic time variation, one obtains one scalar equation and two vector equations:

$$\frac{\partial F_0^0}{\partial t} + \frac{v}{3} \boldsymbol{\nabla}_{\mathbf{r}} \cdot \mathbf{F_0^1} - \frac{1}{v^2} \frac{\partial}{\partial v} \left[\frac{ev^2}{6m} \mathrm{Re}\{\mathbf{E}_p \cdot \mathbf{F_1^1}\} + \frac{ev^2}{3m} (\mathbf{E_s} \cdot \mathbf{F_0^1}) \right]$$

$$= \left(\frac{\partial F_0^0}{\partial t} \right)_c, \tag{4}$$

$$v \boldsymbol{\nabla}_r F_0^0 - \frac{e\mathbf{E_s}}{m} \frac{\partial F_0^0}{\partial v} = -v_c^e \mathbf{F_0^1}, \tag{5}$$

$$j\omega \mathbf{F_1^1} - \frac{e\mathbf{E}_p}{m} \frac{\partial F_0^0}{\partial v} = -\nu_c^e \mathbf{F_1^1}. \tag{6}$$

Here $\mathrm{Re}\{\}$ means *the real part of*, the right-hand side of Eq. (4) denotes the collision operator for the isotropic function F_0^0, and ν_c^e is an effective collision frequency for momentum transfer including both elastic and inelastic contributions [26]. Since $\nu_c^e \gg \tau_e^{-1}$ holds in the whole significant electron energy range, the relaxation of the anisotropic component $\mathbf{F_0^1}$, associated with the density gradients and the space-charge field, occurs much faster than F_0^0, so that $\mathbf{F_0^1}$ may be assumed in quasi equilibrium [$\partial \mathbf{F_0^1}/\partial t = 0$ in Eq. (5)], within the time scale used to study the variations of F_0^0.

Inserting the expressions for $\mathbf{F_0^1}$ and $\mathbf{F_1^1}$ given by Eqs. (5) and (6) into Eq. (4), and neglecting the term in $(\mathbf{E_s} \cdot \mathbf{F_0^1})$ in this latter equation, we obtain the following equation for F_0^0:

$$\frac{\partial F_0^0}{\partial t} - \frac{v^2}{3 \nu_c^e} \nabla_{\mathbf{r}}^2 F_0^0 + \frac{ev}{3m\nu_c^e} \nabla_{\mathbf{r}} \cdot \left(\mathbf{E_s} \frac{\partial F_0^0}{\partial v} \right)$$
$$- \frac{1}{v^2} \frac{\partial}{\partial v} \left[\frac{v^2}{6\nu_c^e} \left(\frac{eE_p}{m} \right)^2 \frac{1}{1+(\omega/\nu_c^e)^2} \frac{\partial F_0^0}{\partial v} \right] = \left(\frac{\partial F_0^0}{\partial t} \right)_c.$$

(7)

The neglect in Eq. (4) of the flux driven in velocity space by the space-charge field (term $\mathbf{E_s} \cdot \mathbf{F_0^1}$), as compared to that driven by the applied field, is justified under present conditions, owing to the relative magnitude of both fields [27]. Nevertheless, $\mathbf{E_s}$ must be kept in Eq. (5), since it nearly balances the diffusion term and causes the total electron particle flow vector

$$\Gamma = \int_0^\infty \mathbf{F_0^1} \frac{4\pi v^3}{3} dv$$

(8)

to become a small quantity [23,24]. Thus, using Eq. (5) in Eq. (8), we obtain

$$\Gamma = -\nabla_{\mathbf{r}}(D_e n_e) - n_e \mu_e \mathbf{E_s},$$

(9)

where

$$D_e = \frac{1}{n_e} \int_0^\infty \frac{v^2}{3\nu_c^e} F_0^0 4\pi v^2 dv$$

(10)

and

$$\mu_e = -\frac{1}{n_e} \int_0^\infty \frac{ev}{3m\nu_c^e} \frac{\partial F_0^0}{\partial v} 4\pi v^2 dv$$

(11)

denote the electron free diffusion coefficient and the dc electron mobility, respectively.

On the other hand, integrating Eq. (7) over all velocities, by multiplying both members of Eq. (7) by the volume element in velocity space $4\pi v^2 dv$ and integrating from 0 to ∞, one obtains the continuity equation for electrons

$$\frac{\partial n_e}{\partial t} - \nabla_{\mathbf{r}}^2 (D_e n_e) - \nabla_{\mathbf{r}} \cdot (n_e \mu_e \mathbf{E_s}) = n_e \langle \nu_{\text{ion}} \rangle - n_e \langle \nu_{\text{rec}} \rangle,$$

(12)

with $\langle \nu_{\text{ion}} \rangle$ and $\langle \nu_{\text{rec}} \rangle$ denoting the energy-averaged frequencies for ionization and electron-ion recombination, respectively. We note that the symbol $\langle \rangle$ denotes the averaging over all velocities. With this notation the free diffusion coefficient given by Eq. (10) is simply written as $D_e = \langle v^2/3\nu_c^e \rangle$. In writing Eq. (12), the term accounting for the flux of electrons in velocity space driven by the applied HF field, that is the fourth term on the left-hand side of Eq. (7), vanishes at both integration limits, as well as the contribution

from all collisions that keep constant the electron number density: that is elastic and inelastic collisions of first and second kind.

A. Discharge

The second and third terms on the left-hand side of Eqs. (7) and (2) may be each quite large, but they nearly cancel each other out under discharge conditions due to the very nature of the ambipolar diffusion regime. This is the reason why both terms are usually neglected at the moment to calculate the EEDF in discharge conditions. Here the EEDF in a low-pressure ($p=2$ and 10 Torr) microwave discharge [$\omega/(2\pi)=2.45$ GHz] in N_2 is obtained by solving the stationary Boltzmann equation for a HF field by assuming $\partial F_0^0/\partial t = 0$ in Eq. (7) (due to the inequality $\omega \gg \tau_e^{-1}$ which is on the basis of the *effective field approximation*), and neglecting terms which depend on position coordinates (*homogeneous Boltzmann equation*). When the diffusion and space-charge field terms are neglected one must also neglect, for consistency, the creation and loss of electrons on the right-hand side of Eq. (7). The Boltzmann equation is hence transformed into a continuity equation for the velocity distribution function, which allows a separable solution of the form $F_0^0(\mathbf{r}, v) = n_e(\mathbf{r}) \times f^0(v)$.

In these conditions, the Boltzmann equation is usually written in the form [28]

$$\frac{dG}{du} = \sum_{ij} [\sqrt{u+u_{ij}} \nu_{ij}(u+u_{ij})f(u+u_{ij}) - \sqrt{u} \nu_{ij} f$$
$$+ \sqrt{u-u_{ij}} \nu_{ji}(u-u_{ij})f(u-u_{ij}) - \sqrt{u} \nu_{ji} f], \quad (13)$$

in which the homogeneous distribution function $f^0(v)$ is replaced with the EEDF, $f(u)$, obeying the normalization condition $\int_0^\infty f\sqrt{u}\,du = 1$, and where $u = \frac{1}{2}mv^2$ denotes the electron energy. The terms inside the brackets on the right-hand side of Eq. (13) take into account the effects of excitation of vibrational and electronic states of N_2 by inelastic collisions (the first and second terms), and of the de-excitation of the vibrational states by electron superelastic collisions (the third and fourth terms), with u_{ij}, ν_{ij}, and ν_{ji} denoting the energy threshold and the inelastic and superelastic collision frequencies, respectively, and $G(u)$ representing the total electron flux in energy space due to the continuous terms in the Boltzmann equation. $G(u)$ is given by the sum of the fluxes driven by the applied HF field, G_E; the elastic collisions, G_c; the electron-electron (e-e) collisions, G_{e-e}; and the inelastic and superelastic collisions of electrons with rotational levels assuming a continuous approximation, G_{rot}. These can be written, respectively, in the forms [28,29]

$$G_E = -\frac{(eE_p)^2}{3m\nu_c^e} \frac{1}{1+(\omega/\nu_c^e)^2} u^{3/2} \frac{df}{du},$$

(14)

$$G_c = -\frac{2m}{M} \nu_c u^{3/2} \left(f + kT_g \frac{df}{du} \right),$$

(15)

$$G_{e\text{-}e} = -2\,\nu_{e\text{-}e} u^{3/2} \left(If + J\frac{df}{du} \right), \qquad (16)$$

$$G_{\text{rot}} = -4B\nu_0 \sqrt{u}f. \qquad (17)$$

In Eqs. (15)–(17), ν_c is the elastic electron-neutral collision frequency for momentum transfer, M is the molecular mass, and T_g is the gas temperature. $\nu_{e\text{-}e}$ is the electron-electron collision frequency given by [23]

$$\nu_{e\text{-}e} = 4\,\pi \left(\frac{e^2}{4\,\pi\epsilon_0 m} \right)^2 \frac{\ln\Lambda}{v^3} n_e, \qquad (18)$$

with ϵ_0 denoting the vacuum permittivity and $\ln\Lambda$ the Coulomb logarithm. I and J are two integral functions of $f(u)$ known as Spitzer's integrals [23], $B(=2.5\times10^{-4}$ eV) is the rotational constant in N_2, and $\nu_0 = n_0\sqrt{2u/m}\,\sigma_0$ is a frequency for rotational exchanges induced by electron impact, including both inelastic and superelastic processes, obtained using the continuous approximation [29], in which n_0 is the gas density and $\sigma_0 = 8\,\pi q^2 a_0^2/15$, with q ($=1.01$ in N_2) denoting the electric quadrupole moment in units of ea_0^2 and a_0 the Bohr radius.

Equation (13) is solved coupled to a system of rate balance equations for the vibrational and electronic states of N_2 and $N(^4S)$ atoms, and N_2^+ and N_4^+ ions, in order to account for superelastic collisions of electrons with vibrationally excited molecules $N_2(X\ ^1\Sigma_g^+,v)$. Moreover, the sustaining HF electric field is self-consistently determined using the requirement that under steady-state conditions the total rate of ionization must compensate exactly for the rate of electron losses by diffusion, under the effects of a space-charge field, plus electron-ion recombination [30,31]. We note that the continuity equation for electrons is no longer implicit in Eq. (13), so that the former must be taken independently for the purposes of determining the electric field necessary for discharge maintenance. For this purpose, the total ionization rate must include besides the processes of direct electron impact ionization on $N_2(X,v)$ molecules and electron stepwise ionization on $N_2(A\ ^3\Sigma_u^+)$ and $N_2(a'^1\Sigma_u^-)$ states, as well as the processes of associative ionization due to collisions between metastable states: that is, by collisions $N_2(A)+N_2(a')$ and $N_2(a')+N_2(a')$; see Refs. [30,31] for details.

B. Post-discharge

Let us now consider the electron distribution function in the earlier instants of the afterglow of a stationary discharge by assuming a zero electric field at $t=0$ in Eq. (7), using the stationary distribution in the discharge as the initial condition. This is indeed an approximation, since E_p cannot drop to zero instantaneously [20,32]. In this case, the nonconservative terms for the electron density, associated with electron losses by electron-ion recombination and diffusion in the presence of the space-charge field E_s, should now be included, with the effects produced by the field E_s being progressively decreased as the time evolves.

The time-dependent Boltzmann equation in the form expressed by Eq. (7) is difficult to solve, even numerically, due to the presence of the space-charge field term and of the dependence of F_0^0 on the configuration and velocity spaces. As a matter of fact, in order to determine E_s self-consistently, Poisson's equation must be used, coupled to the continuity and momentum transport equations for both electrons and ions. This task involves a great deal of computational work, and is hence beyond the scope of the present paper. Here we are mainly interested in deriving a self-contained equation to treat this problem, which may be used for practical purposes in different situations.

With this aim, we note that the transition from ambipolar to free diffusion, as the plasma conductivity decreases, was studied in Ref. [23] by solving a set of equations formed by Poisson's equation, and by continuity and momentum transfer equations for both electrons and ions, making two simple assumptions: congruence $\mathbf{\Gamma_e}=\mathbf{\Gamma_i}$ and proportionality $\mathbf{\nabla_r}n_e/n_e = \mathbf{\nabla_r}n_i/n_i$. In Ref. [23] it was shown that the total electron particle flow vector $\mathbf{\Gamma}$ given by Eq. (9) may be replaced by the equation

$$\mathbf{\Gamma} = -D_{se}\mathbf{\nabla}_r n_e, \qquad (19)$$

where D_{se} denotes an effective diffusion coefficient for electrons, under the presence of the space-charge field, given by

$$D_{se} = D_a \frac{D_e + \Lambda^2 e n_e \mu_e/\epsilon_0}{D_a + \Lambda^2 n_e \mu_e/\epsilon_0}. \qquad (20)$$

Here $D_a \sim (\mu_i/\mu_e)D_e$ is the ambipolar diffusion coefficient, μ_i is the ion mobility, and $\Lambda = R/2.405$ is the characteristic diffusion length for a cylindrical container of radius R, obtained by replacing $\mathbf{\nabla_r^2}n_e$ with $\sim -n_e/\Lambda^2$, which is consistent with the assumption that n_e vanishes at the wall. The remaining quantities in Eq. (20) have been previously defined. In the limit $\lambda_D \ll \Lambda$, with $\lambda_D = \sqrt{\epsilon_0 u_k/e^2 n_e}$ denoting the electron Debye length and $u_k = eD_e/\mu_e$ the characteristic energy, we obtain $D_{se}\to D_a$, whereas we have $D_{se}\to D_e$ for $\lambda_D \gg \Lambda$. Equation (19) hence allows one to cover the bridge between nearly ambipolar diffusion (in the earlier and intermediate instants of the afterglow) and free diffusion (in the late afterglow) by considering the decreasing of n_e and the variation of both D_e and μ_e.

Keeping in mind that, with the concept of effective diffusion coefficient, the integration of both members of Eq. (7) over all velocities gives the continuity equation

$$\frac{\partial n_e}{\partial t} + D_{se}\frac{n_e}{\Lambda^2} = n_e\langle\nu_{\text{ion}}\rangle - n_e\langle\nu_{\text{rec}}\rangle, \qquad (21)$$

we will return to the Boltzmann equation and assume that the second and third terms on the left-hand side of Eq. (7) may be replaced by a sole term accounting for diffusion of electrons under the presence of a space-charge field. With this assumption the time-dependent Boltzmann equation, able to describe the evolution of the EEDF in the afterglow, may be written in the form

$$\frac{\partial F}{\partial t} + \frac{2}{3m} \frac{u}{\nu_c^e \Lambda^2} \frac{D_{se}}{D_e} F + \frac{1}{\sqrt{u}} \frac{\partial G}{\partial u}$$

$$= \frac{1}{\sqrt{u}} \sum_{ij} \left[\sqrt{u+u_{ij}} \nu_{ij}(u+u_{ij}) F(u+u_{ij}) - \sqrt{u}\, \nu_{ij} F \right.$$

$$\left. + \sqrt{u-u_{ij}} \nu_{ji}(u-u_{ij}) F(u-u_{ij}) - \sqrt{u}\, \nu_{ji} F \right] - \nu_{\text{rec}} F. \tag{22}$$

Under the present formulation, once the EEDF and the electron density in the discharge are known, the EEDF in the post-discharge $F(u,t)$ can be obtained by solving Eq. (22), using the stationary distribution $f(u)$ and the electron density in the discharge as initial conditions, $F(u,0) = n_e f(u)$, and assuming a zero electric field [$G_E = 0$ in Eq. (14)]. The EEDF in the post-discharge, with the normalization $\int_0^\infty F \sqrt{u}\, du = n_e(t)$, can then be calculated from Eq. (22), considering the decreasing of $n_e(t)$ and the time variation of D_e and μ_e in D_{se} at each instant of the afterglow. The last term on the right-hand side of Eq. (22) accounts for the electron-loss process of dissociative recombination, with a frequency ν_{rec}, whose cross section was taken from Ref. [33]. The reader should refer to previous papers [30,31] for further details of collisional data in N_2. On the other hand, the production of secondary electrons by ionization has been neglected in the afterglow, since the EEDF is rapidly depleted in the high-energy range in a very short time, $\sim 10^{-8} - 10^{-7}$ s, as we will show below. Hence the ionization is considered here as any other inelastic process, assuming the energy loss of primary electrons only. In conclusion, Eq. (22) should not be considered as a rigorous equation to describe the time evolution of the EEDF in the afterglow, but just as an approximate equation than can be used to avoid the complexity embodied in Eq. (7), since the latter contains a double dependence on configuration and velocity spaces.

Finally, the self-consistent determination of the EEDF should couple Eq. (22) with a system of time-dependent kinetic master equations for the vibrational levels $N_2(X\ ^1\Sigma_g^+, v)$, taking into account electron-vibration (e-V), vibration-vibration (V-V), and vibration-translation (V-T) energy exchange processes [9,30], in order that the decrease of the concentrations $[N_2(X,v)]$ along the post-discharge may be considered in Eq. (22) in terms associated with inelastic and superelastic e-V collisions. Here, in order to simplify this problem, we assume that the concentrations of $N_2(X,v)$ molecules, that is, the so-called vibrational distribution function (VDF), do not vary significantly in the post-discharge, which is not absolutely true as shown below, since the vth levels continue to be populated in the afterglow not only by e-V processes but also by nonresonant V-V energy exchanges [9,12]. The latter due to the so-called V-V pumping up effect, first pointed out in Ref. [12] and also analyzed in the detail for this very situation in Ref. [9]. Future work will consider the coupled evolution of both the EEDF and the VDF in the post-discharge, limiting us here to an analysis of the influence of the transition from ambipolar to free diffusion regimes on the EEDF, and on related electron energy-

averaged quantities obtained from the EEDF, such as the electron density, electron mean energy, electron transport parameters, and various electron rate coefficients for electronic and vibrational excitation either by direct electron impact or stepwise excitation.

III. RESULTS AND DISCUSSION

The calculations in this paper were carried out for typical operating conditions of a flowing microwave discharge in pure N_2 [4–7]. In particular, we consider a microwave discharge at $\omega/(2\pi) = 2.45$ GHz in a Pyrex tube of inner radius $R = 0.8$ cm; two values of pressure $p = 2$ and 10 Torr; a unique value of the electron density $n_e = 5 \times 10^{11}$ cm^{-3}, which is usually modified in an experiment by varying the injected microwave power; and a typical constant value of the gas temperature at present conditions $T_g = 1000$ K [9]. At $p = 2$ Torr, for example, we obtain the following discharge parameters using the present kinetic model: $E_e/n_0 = 1.36 \times 10^{-15}$ V cm^2 for the reduced effective electric field necessary for sustaining the HF discharge [27,28], $dP_{\text{abs}}/dz = 33$ W cm^{-1} for the mean input power absorbed per unit length, $T_v = 21\,100$ K (that is, $kT_v = 1.82$ eV) for the vibrational temperature of the lowest vth levels of the VDF, and $[N(^4S)]/n_0 = 0.154$ for the fractional concentration of $N(^4S)$ atoms. It is worth noting at this point that the VDF is very distant from a Boltzmann distribution, so that the temperature T_v is defined here as the characteristic vibrational temperature of the Treanor-like distribution that best fits the calculated VDF in the lowest four vth levels. Although the predicted value $T_v = 21\,100$ K seems to be very high, this is not the case in a microwave discharge at $\omega/(2\pi) = 2.45$ GHz with the present choice of input parameters [9], since the mean power absorbed from the field per electron $\theta = (dP_{\text{abs}}/dz)/n_e \pi R^2$ reaches $\sim 2 \times 10^8$ eV s^{-1}.

Once the EEDF in the discharge $f(u)$ is obtained, the relaxation of $F(u,t)$ is analyzed by solving Eq. (22), with $E_e/n_0 = 0$, and by setting $F(u,0) = n_e \times f(u)$ as the initial condition. With this aim, Eq. (22) is transformed to a set of coupled ordinary differential equations by a finite differencing of the electron energy axis into n cells of width Δu, using a scheme close to that reported in Ref. [34], and employing the following algorithm for time-evolution:

$$\sqrt{u}\,\underline{\mathbf{I}} \cdot \mathbf{F}(t+\Delta t) = (\Delta t \underline{\mathbf{A}} + \sqrt{u}\,\underline{\mathbf{I}}) \cdot \mathbf{F}(t). \tag{23}$$

Here $\underline{\mathbf{I}} = \delta_{ij}$ is the identity matrix, $\sqrt{u}\,\underline{\mathbf{I}} = \sqrt{u_i}\,\delta_{ij}$, with $u_i = (i-1/2)\Delta u$ denoting the energy in the middle of the cell i of energy grid, Δt is the time step, $\mathbf{F}(t)$ is the EEDF at instant t, and $\underline{\mathbf{A}}$ is a matrix of coefficients obtained from finite differencing all terms of Eq. (22).

The electron density is updated during the time-evolution process in the term taking into account e-e collisions, in $\nu_{\text{rec}}(t) = n_i(t)\sqrt{2u/m}\,\sigma_{\text{rec}}$ (with σ_{rec} denoting the electron-ion recombination cross section and where it is assumed $n_i = n_e$ at each instant), and in D_{se}/D_e given by Eq. (20). In this latter equation, D_e and μ_e are also updated at each instant. Equation (23) evolves with an initial time-step $\Delta t \sim 10^{-10}$ s
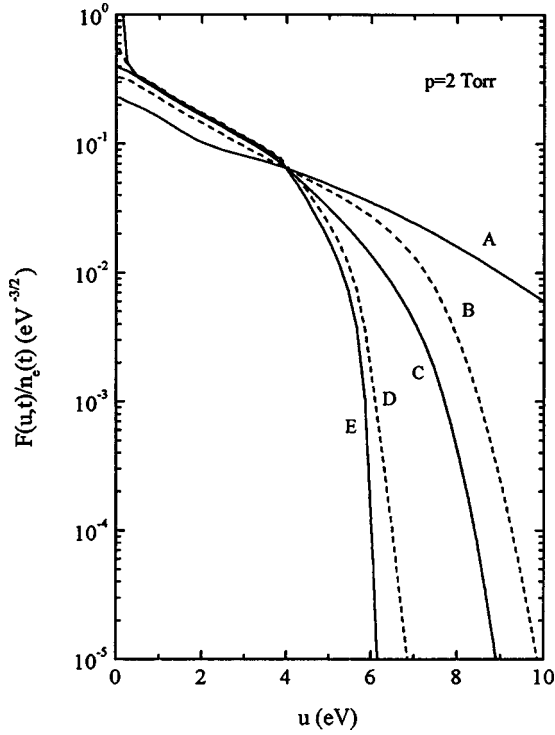
FIG. 1. EEDF calculated in the post-discharge of an $\omega/(2\pi)$ $= 2.45$ GHz microwave discharge in N_2, with $p = 2$ Torr and $n_e(0) = 5 \times 10^{11}$ cm^{-3}, for the following instants in the afterglow: (A) $t = 0$, (B) 10^{-7} s, (C) 10^{-5} s, (D) 10^{-4} s, (E) 3.2×10^{-4} s.

for the first iterations and then a predictor-corrector method (Adams-Bashforth method) is used for adjusting the stepsize [35]. We note that in a self-consistent determination of the EEDF, Eq. (23) should be solved together with a system of kinetic master equations for the vibrational levels $N_2(X {}^1\Sigma_g^+, v)$, that is with a system of equations describing the time-evolution of the VDF, in order that the effect of e-V superelastic collisions may also be updated. Here, for the sake of simplicity, we assume that the concentrations of $N_2(X, v)$ do not vary significantly, which is not absolutely true for the manifold of vth levels as it can be seen in Ref. [9]. The full self-consistency between the EEDF and VDF will be achieved in a future publication.

Figure 1 shows the EEDF calculated at different instants ($t = 0 - 3.2 \times 10^{-4}$ s) in the afterglow of a HF discharge with $p = 2$ Torr. The rapid depletion of the high-energy tail of the EEDF at the earlier instants of the afterglow ($t < 10^{-7}$ s) occurs as a result of electron inelastic collisions. The EEDF is calculated in the presence of e-e collisions, since during the relaxation process the EEDF goes toward the low-energy part of the distribution, where the Coulomb cross section, which sharply increases with decreasing electron energy, plays an important role in affecting the EEDF. Figure 2 shows the EEDF calculated with the inclusion (full curves) and in the absence of e-e collisions (broken curves), at $t = 10^{-7}$, 10^{-6}, 10^{-5}, and 10^{-4} s. The effects produced by e-e collisions on the EEDF are particularly important at intermediate instants $\sim 10^{-5}$ s producing a large increase in the

tail of the EEDF, typically for energies larger than ~ 6 eV and smoothing the peak near $u \sim 0$.

Although the EEDF is largely modified at short times as small as 10^{-7} s Fig. 3 shows that the electron density remains practically unchanged up to $t \sim 10^{-5}$ s due to the large characteristic times for electron losses by ambipolar diffusion, so that within the time interval of Figs. 1 and 2, the EEDF is consistent with the normalization condition $\int_0^\infty F(u, t) \sqrt{u} \, du = n_e \sim$ const. Figure 3 reports the values for $n_e(t)$ calculated from Eq. (22), in which a transition from ambipolar to free diffusion regimes is considered (curve A), as well as the values obtained when free diffusion of electrons is assumed during the whole relaxation process [i.e., assuming $D_{se}/D_e = 1$ in Eq. (22), curve B]. For comparison, we also report the values of $n_e(t)$ in the absence of e-e collisions, but considering the transition from ambipolar to free diffusion (curve C).

As expected, n_e falls sharply at $t \sim 10^{-7} - 10^{-6}$ s as the electron diffusion occurs without the presence of a space-charge field (curve B in Fig. 3), whereas the inclusion or a absence of e-e collisions produce only minor modifications on n_e (curves A and C). The behavior exhibited by $n_e(t)$ in curves A and C essentially results from the fact of the effective diffusion coefficient D_{se} remains practically unchanged up to $t \sim 3 \times 10^{-4}$ s, with $D_{se} \sim D_a$, the instant at which it increases sharply due to the diminution of n_e. Figure 4 shows the ratio D_{se}/D_e, given by Eq. (20), calculated under the same conditions as before, with the inclusion (curve A) and in the absence (curve B) of e-e collisions. The free diffusion is completely achieved at $t \sim 4 \times 10^{-4}$ s.

In contrast to the situation of n_e, the reduction of the rate coefficients for excitation by electron impact of N_2 electronic states from the electronic ground-state $N_2(X {}^1\Sigma_g^+)$ occurs at considerably shorter times. Figures 5(a) and 5(b) show the temporal evolution of the rate coefficients for excitation of $N_2(A {}^3\Sigma_u^+)$, $N_2(B {}^3\Pi_g)$ and $N_2(C {}^3\Pi_u)$ triplet states [Fig. 5(a)] and for excitation of the singlet states $N_2(a' {}^1\Sigma_u^-)$ and $N_2(a {}^1\Pi_g)$ plus ionization [Fig. 5(b)], at the same working conditions as before, and when the transition $D_a \rightarrow D_e$ is considered together with e-e collisions. The present calculations reveal the existence of a decrease of about two orders of magnitude in the rate coefficients for excitation of $N_2(A)$ and $N_2(B)$ states from $N_2(X)$, in the range t $\sim 10^{-9} - 10^{-6}$ s, followed by a region extended up to $t \sim 5 \times 10^{-5}$ s, where the decrease is much less pronounced. For the other states the decrease is always faster.

Figures 6(a) and 6(b) show, for comparison, the calculated rate coefficients for excitation of $N_2(A)$ and $N_2(B)$ states, respectively, using (i) our reference model [curves A, identical to Fig. 5(a)], (ii) assuming $D_{se}/D_e = 1$ during the whole relaxation process (curves B), and (iii) in the absence of e-e collisions but including the transition from ambipolar to free diffusion regimes (curves C). Figures 6(a) and 6(b) clearly show that as free diffusion is assumed, at the beginning of the afterglow, an extremely fast decrease is obtained for the electron rate coefficients, which is the origin of the assumption usually made for the neglect of electron impact process in the post-discharge. However, as the transition
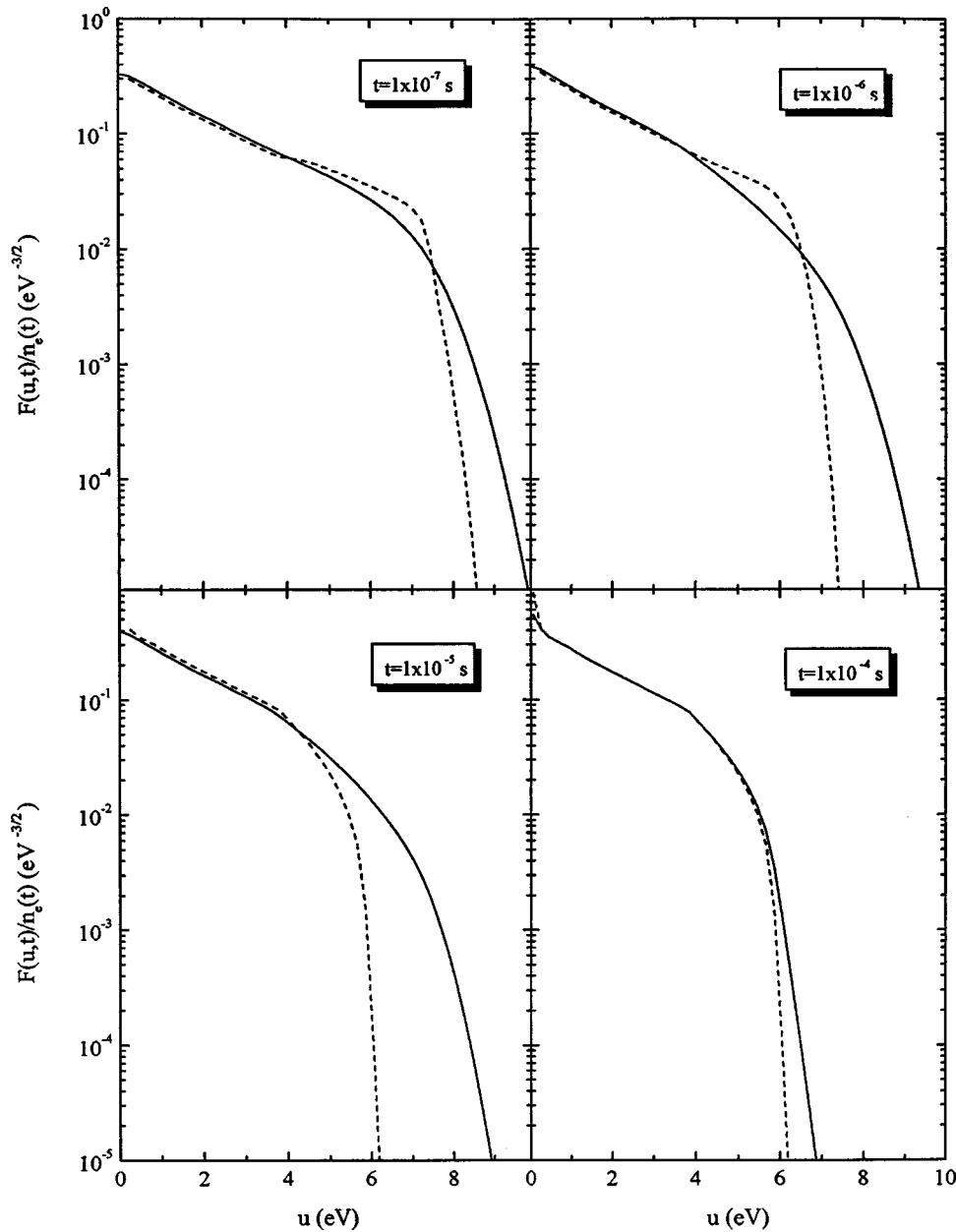
FIG. 2. EEDF calculated in the same conditions as in Fig. 1, with the inclusion (full curves) and in the absence (broken curves) of e-e collisions, for the instants $t = 10^{-7}$, 10^{-6}, 10^{-5}, and 10^{-4} s. The full curves are the same as in Fig. 1.

$D_a \rightarrow D_e$ is considered, the rate coefficient $C_{X,A}$ presents a nearly constant value of about two orders of magnitude smaller than that calculated in the discharge, in a broad time interval $t \sim 5 \times 10^{-7}$–5×10^{-5} s, so that, during the relaxation of some heavy active species produced in the discharge, the excitation by electron impact in the post-discharge is not absolutely vanishing at all. Finally, Fig. 6(a) also shows for case (iii) that a quasistationary state is achieved between the EEDF and VDF at $\sim 5 \times 10^{-6}$ s, in which the superelastic collisions of electrons with vibrationally excited molecules $N_2(X,v)$ compensate for the inelastic vibrational losses [12]. This effect only slightly appears in our reference case (i) at $\sim 2 \times 10^{-4}$ s, that is, just before the sharp decrease dictated by the change in the diffusion regime. On the other hand, the magnitude of the rate coefficients for excitation of $N_2(B)$ is always too small in order that this effect may be observed in Fig. 6(b).

Figures 5 and 6 show that even in the case where the transition from ambipolar to free diffusion is taken into account, the electron rate coefficients for excitation, although not absolutely vanishing, are sufficiently small to validate the assumption usually made for the neglect of the processes by electron impact in a post-discharge. However, the same conclusion cannot be inferred in the case of excitation by slow electrons, e.g., for stepwise excitation of $N_2(B\ ^3\Pi_g)$ and $N_2(C\ ^3\Pi_u)$ states from $N_2(A\ ^3\Sigma_u^+)$. Figure 7 shows the rate coefficients of these processes calculated using the cross section data [36], with the same notations as in Fig. 6. The rate coefficient for excitation $N_2(A) \rightarrow N_2(B)$ induced by electron impact remains almost constant in the time interval $t \sim 10^{-9}$–10^{-4} s, while that associated with the transition $N_2(A) \rightarrow N_2(C)$ is reduced by a factor of 10 when the time evolves up to $\sim 5 \times 10^{-5}$ s.
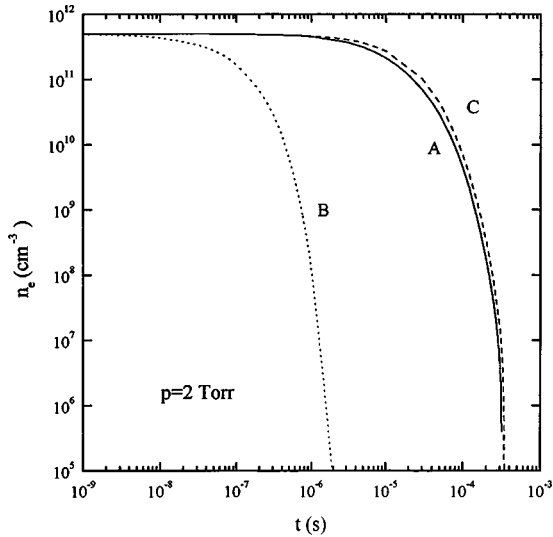
FIG. 3. Temporal evolution of the electron number density in a N_2 post-discharge, calculated for the same conditions as in Fig. 1, using our reference model (A), assuming free diffusion of electrons during the whole relaxation process (B), and neglecting e-e collisions (C).

Experimental evidence of the existence of non-negligible electron impact processes in a N_2 afterglow was observed in Refs. [22,37]. In the post-discharge of a N_2 pulsed rf discharge [22], it was shown that the $N_2(C)$ state continues to be populated by collisions of low-energy electrons (energies typically of the order ~ 4 eV) on $N_2(A)$, up to afterglow times as large as ~ 1 ms. On the other hand, it was also pointed out in Ref. [37] that a quite probable reason for the disagreement between the calculated and measured fluorescences from $N_2(B)$, in the early afterglow ($t < 10^{-4}$ s) of a
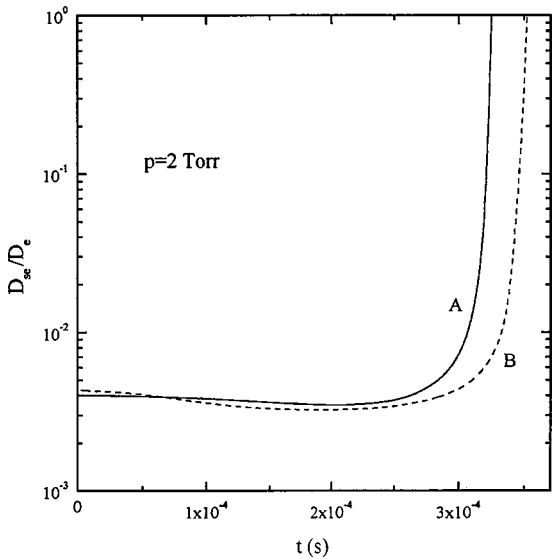
FIG. 4. Temporal evolution of the ratio of the effective electron diffusion coefficient to the free diffusion coefficient in a N_2 post-discharge, for the same conditions as in Fig. 1, including (A) and neglecting (B) e-e collisions. The nearly flat region for D_{se}/D_e corresponds to ambipolar diffusion.
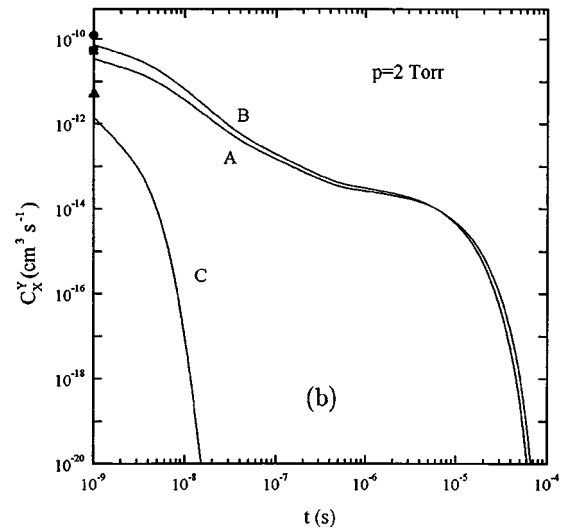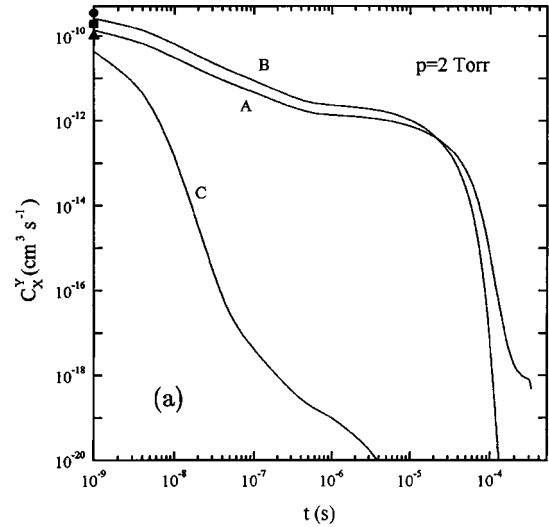
FIG. 5. Temporal evolution of the electron rate coefficients for excitation of $N_2(A)$, $N_2(B)$, and $N_2(C)$ states [curves $A-C$ in Fig. 5(a)], and for excitation of $N_2(a')$ and $N_2(a)$ states plus ionization [curves $A-C$ in Fig. 5(b)], calculated in a N_2 afterglow for the same conditions as in Fig. 1, using our reference model for electron diffusion and including e-e collisions. The symbols represent the rate coefficients in the discharge ($t=0$).

N_2 pulsed discharge, may be associated with neglecting, in the model used in that paper, of $N_2(B)$ excitation by the impact of slow electrons on $N_2(A)$.

Figure 8 shows the electron rate coefficients for vibrational excitation (0-v transitions) and de-excitation (v-0) of $N_2(X\ ^1\Sigma_g^+,v)$ levels (with $v=1$, 3, and 5), for the same working conditions as before, in the case of our reference model in what concerns the effects of diffusion (that is, including the transition of diffusion regime $D_a \rightarrow D_e$). During the relaxation process, the electrons tend to concentrate in the low-energy part of the EEDF, which causes an increase in the electron rate coefficients for vibrational excitation, owing to the relatively low-energy thresholds for these processes. Thus, the decrease of the e-V populating rates in the post-discharge, $R_v \sim n_e[N_2(X,0)]C_{0,v}$, just occurs at the mo-
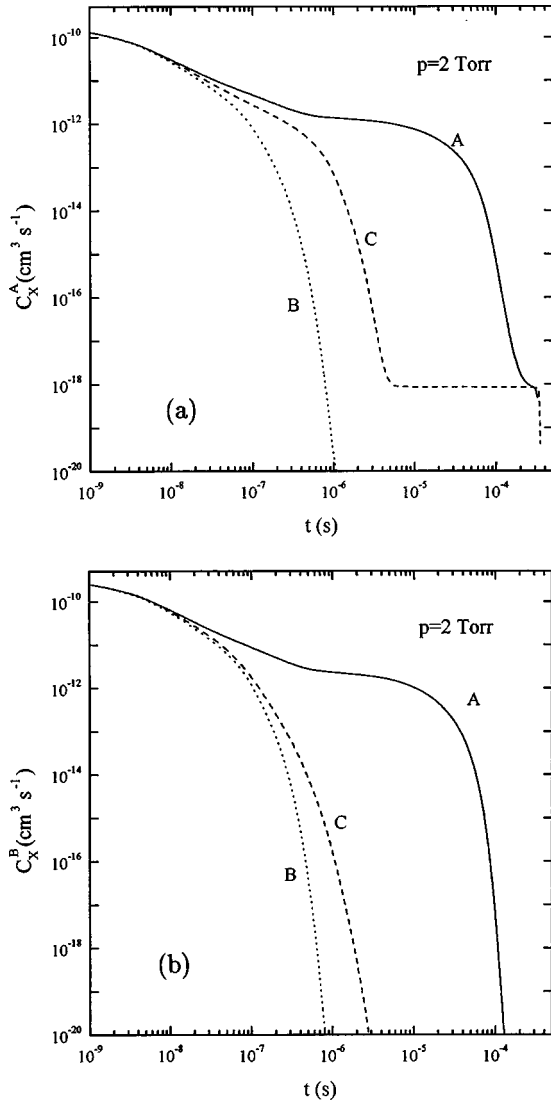
(a)

(b)

FIG. 6. Temporal evolution of the electron rate coefficients for excitation of $N_2(A)$ [Fig. 6(a)] and $N_2(B)$ [Fig. 6(b)] states, calculated in the same conditions as in Fig. 1, using our reference model (A), assuming free diffusion of electrons only (B), and neglecting e-e collisions (C).

ment when the electron density starts to decrease, that is at $t\sim 10^{-5}$ s (see Fig. 3), and not as a consequence of the decrease of the rate coefficients for vibrational excitation $C_{0,v}$. It should therefore be expected that the VDF will continue to be strongly populated in early and intermediate instants of the afterglow, not only in the higher vth levels as a result of the V-V (vibrational-vibrational) pumping up effect discussed in Ref. [9], which is a consequence of the anharmonicity of the potential curve of $N_2(X)$ molecules, but also in the lower levels due to the increase of e-V rate coefficients.

Figures 9 and 10 show, for the same cases as in Figs. 6 and 7, the time-evolution of the electron kinetic temperature defined as $kT_e = \frac{2}{3}\langle u \rangle$, with $\langle u \rangle$ denoting the electron average energy, and the rate coefficient for electron-ion recombination $\alpha = \langle \nu_{rec} \rangle / n_i = \langle \sqrt{2u/m}\,\sigma_{rec} \rangle$, calculated using the cross section data [33]. The global behavior exhibited by kT_e is quite similar to that shown by the rate coefficients for exci-
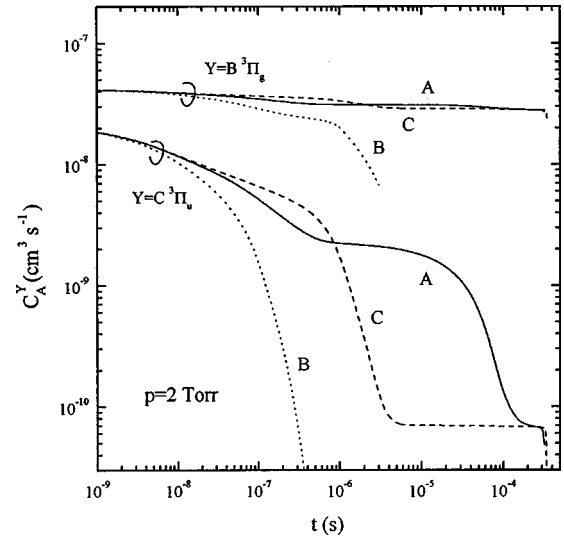

FIG. 7. Temporal evolution of the electron rate coefficients for stepwise excitation of $N_2(B)$ and $N_2(C)$ states from $N_2(A)$, calculated in a N_2 afterglow for the same conditions as in Fig. 1, using our reference model (A), assuming free diffusion of electrons only (B), and neglecting e-e collisions (C).

tation of $N_2(A\ ^3\Sigma_u^+)$ and $N_2(B\ ^3\Pi_g)$ states, with an initial rapid decrease in the first instants of the afterglow up to $t\sim 10^{-6}$ s followed by a slowly decreasing region in the time interval 10^{-6}–5×10^{-5} s. In this latter time-interval the EEDF and VDF are in quasiequilibrium through inelastic and superelastic e-V collisions; hence $T_e\sim T_v$ [15]. On the other hand, the steep increase of the electron-ion recombination rate coefficient as t evolves is an obvious consequence of the modifications produced on the EEDF along the relaxation process, since the depletion of the high-energy tail of the distribution gives way, by normalization, to the appearance of a sharp peak centered at $u\sim 0$. The progressive modi-
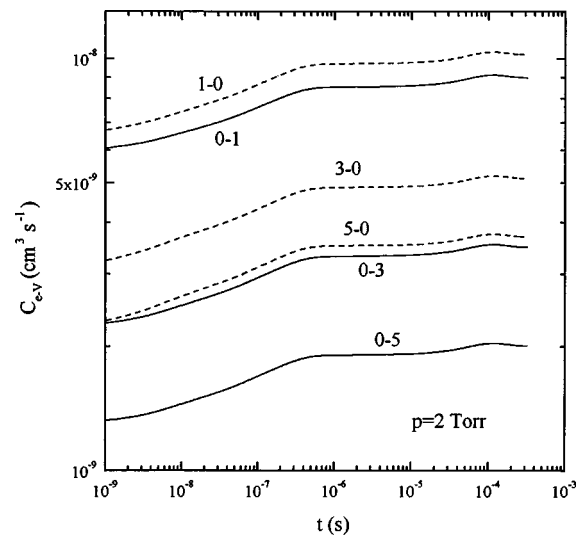

FIG. 8. Temporal evolution of the electron rate coefficients for vibrational excitation (full curves) and de-excitation (broken curves), associated with $(0$-$v)$ and $(v$-$0)$ transitions, calculated in a N_2 afterglow for the same conditions as in Fig. 1.
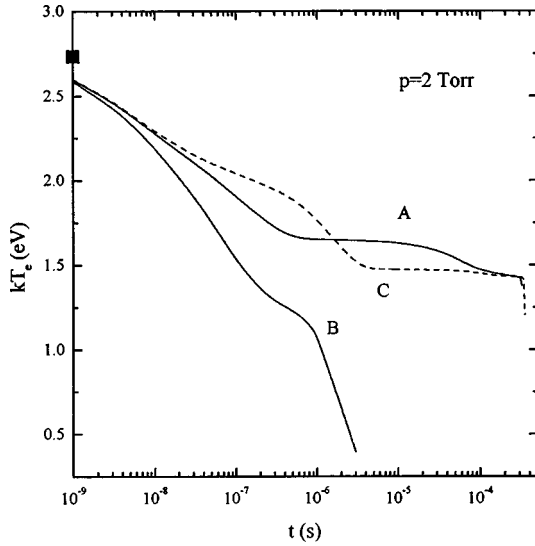
FIG. 9. Temporal evolution of the electron kinetic temperature in eV, in a N_2 afterglow for the same conditions as in Fig. 1, using our reference model (A), assuming free diffusion of electrons only (B), and neglecting e-e collisions (C). The symbol denotes the value of kT_e in the discharge ($t=0$).

fications of the shape of the EEDF, together with the fact that the recombination cross section presents a dependence on the electron energy with the form $\sigma_{\rm rec} \sim u^{-1}$ [38], produce the changes shown in Fig. 10 for the rate coefficient α.

Up to now, only results for $p=2$ Torr have been presented. By inspection of Eq. (22), we observe that the frequency for electron losses by diffusion under the presence of the space-charge field follows the law n_0^{-1}, according to

$$\nu_{\rm dif} = \frac{2}{3m} \frac{u}{n_0 \sqrt{2u/m} \sigma_c^e \Lambda^2} \frac{D_{se}}{D_e}, \tag{24}$$
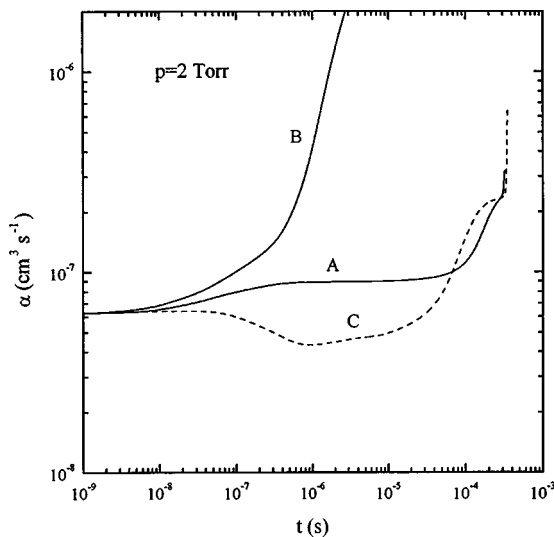

FIG. 10. Temporal evolution of the electron rate coefficient for electron-ion recombination, in a N_2 afterglow for the same conditions as in Fig. 1, using our reference model (A), assuming free diffusion of electrons only (B), and neglecting e-e collisions (C).
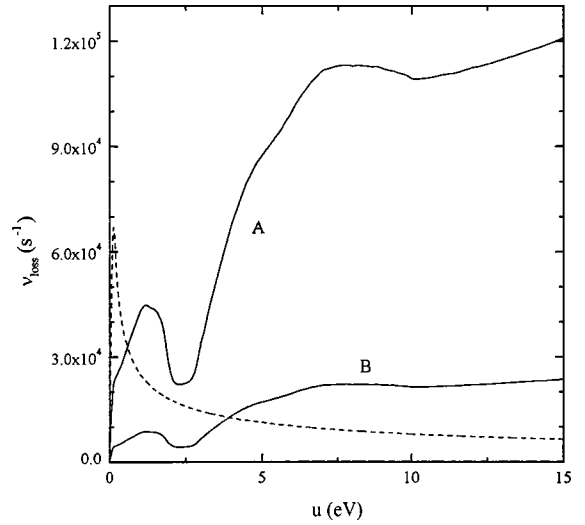

FIG. 11. Frequencies for electron losses by diffusion under the effects of the space-charge field (full curves) and by electron-ion recombination (broken curves), calculated in an $\omega/(2\pi) = 2.45$ GHz microwave discharge in N_2, with $p=2$ Torr (A) and 10 Torr (B), and for $n_e=n_i=5\times10^{11}$ cm^{-3}, $R=0.8$ cm, and $T_g = 1000$ K.

where σ_c^e denotes the effective cross section for momentum transfer. Figure 11 reports, for comparison, the frequencies for electron losses by diffusion, $\nu_{\rm dif}$, and by volume recombination,

$$\nu_{\rm rec} = n_i \sqrt{\frac{2u}{m}} \sigma_{\rm rec}, \tag{25}$$

against the electron energy, calculated at the beginning of the afterglow ($t=0$), for $p=2$ and 10 Torr keeping all other input parameters as before [$\omega/(2\pi)=2.45$ GHz, $n_e=n_i=5\times10^{11}$ cm^{-3}, $R=0.8$ cm, and $T_g=1000$ K]. Figure 11 shows that the main electron-loss mechanism is diffusion except in a narrow region near $u\sim0$, where the electron-ion recombination dominates. On the other hand, the frequency for electron diffusion decreases as p increases from 2 to 10 Torr, approximately with $\sim p^{-1}$, since the modifications on $\nu_{\rm dif}$ produced by variations on D_{se}/D_e are always negligibly small.

The changes on $\nu_{\rm dif}$ with pressure fully interpret the temporal evolution of the electron density in the afterglow of a 2.45-GHz microwave discharge, at $p=2$ and 10 Torr, shown in Fig. 12. The sharp decrease of $n_e(t)$ is considerably shifted to a longer instant $t\sim1$ ms, as the pressure increases from 2 to 10 Torr. As a result of the modifications that occur in $n_e(t)$, the change from ambipolar to free diffusion regimes is also retarded from 2×10^{-4} to $\sim10^{-3}$ s, as p varies between these two values of pressure; see Fig. 13.

The present results are qualitatively in line with the measurements realized in Ref. [21] using the breakdown time delay technique, in which it was observed, in a setup different from ours, although at $p=5$ Torr, that a rapid transition from ambipolar to free diffusion is needed at $t\sim20$ ms to fit the data. This apparent increase of the instant at which the transition from ambipolar to free diffusion occurs is surely
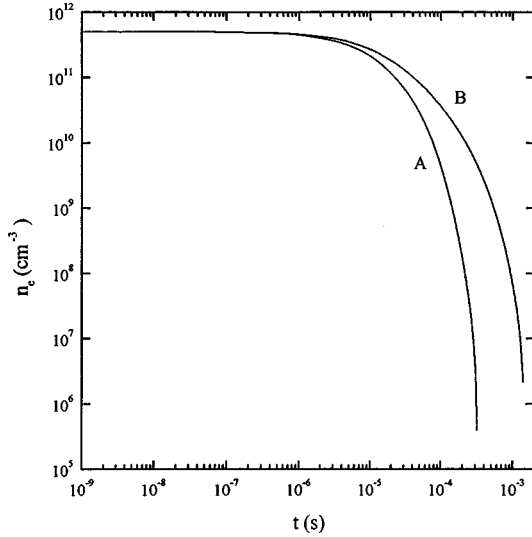
FIG. 12. Temporal evolution of the electron number density in the post-discharge of an $\omega/(2\pi)=2.45$ GHz microwave discharge in N_2, with $n_e(0)=5\times10^{11}$ cm^{-3}, $R=0.8$ cm, and $p=2$ Torr (A) and 10 Torr (B).

FIG. 14. Temporal evolution of the electron kinetic temperature in eV, in a N_2 post-discharge for the same conditions and notations as in Fig. 12. The symbols denote the values of kT_e in the discharge $(t=0)$.

associated with a large tube radius in the conditions of the experiment [21]. The memory curves in Ref. [21] were obtained for a gas tube made of molybdenum glass with a volume of $V=160$ cm^3 and an area $S_W=180$ cm^2, which allows $R\sim1.8$ cm in the case of a cylindrical tube, whereas in the conditions of the present paper we have $R=0.8$ cm. Since the transition of the diffusion regime occurs when the inequality $\lambda_D\sim\Lambda$ holds, a larger tube radius implies a smaller electron density $n_e(t)$; consequently the transition point arises at a larger time.

Figure 14 shows the time relaxation of the electron kinetic temperature in the afterglow of a HF discharge at $p=2$ and 10 Torr, keeping all other conditions as before. The reduction of kT_e with increasing gas pressure results from the decrease in the reduced effective electric field for discharge
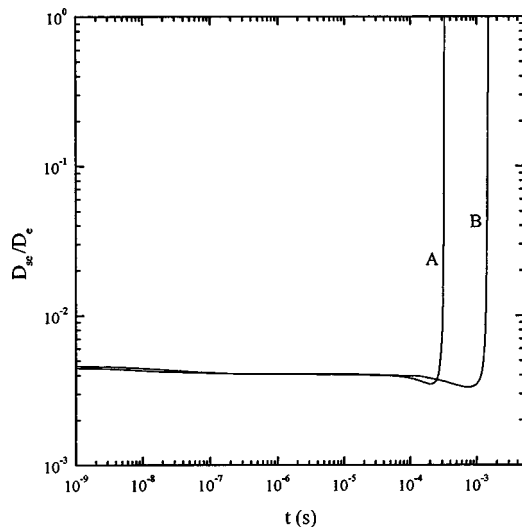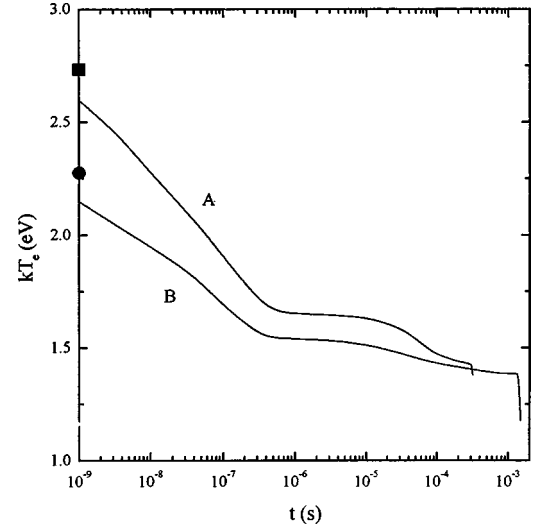

FIG. 13. Temporal evolution of the ratio of the effective electron diffusion coefficient to the free diffusion coefficient in a N_2 post-discharge, for the same conditions and notations as in Fig. 12.

sustaining, E_e/n_0. This parameter decreases from 1.36 $\times10^{-15}$ down to 7.7×10^{-16} V cm^2, as p increases within this range of values. In both cases, kT_e first decreases with a slope not very pronounced, up to $t\sim3\times10^{-7}$ s, followed by an extended region where the electron temperature remains practically constant due to the achievement of a quasistationary state between the EEDF and the VDF, dictated by the compensation of inelastic and superelastic e-V processes. At the higher value $p=10$ Torr, we have $kT_e\sim1.5$ eV in a relatively extended region $t\sim3\times10^{-7}-10^{-3}$ s.

Finally, Fig. 15 shows, for completeness, the EEDF calculated at $p=10$ Torr for different instants of the afterglow, in the time interval $(0-1.4)\times10^{-3}$ s, while in Fig. 16 we report, for the same value of pressure, the time evolution of the electron rate coefficients for excitation of $N_2(A\ ^3\Sigma_u^+)$, $N_2(B\ ^3\Pi_g)$, and $N_2(C\ ^3\Pi_u)$ states, from the electronic ground state $N_2(X\ ^1\Sigma_g^+)$. Both figures are obtained considering the transition from ambipolar to free diffusion regimes in the Boltzmann equation, and taking into account e-e collisions. The general trends exhibited here are not very different from those previously shown in Figs. 1 and 5(a) for $p=2$ Torr. The main difference between 2 and 10 Torr occurs in the high-energy tail of the EEDF at intermediate instants, $t\sim10^{-7}-10^{-5}$ s, in which a more pronounced decrease is observed at $p=10$ Torr, leading to a steeper decrease of the electronic rate coefficient for excitation of $N_2(C)$.

IV. CONCLUDING REMARKS

An important aspect of the present paper is that to our knowledge it is the first time that the relaxation of the EEDF in a N_2 afterglow has been analyzed by solving the Boltzmann equation, taking into account the progressive reduction of space-charge field effects, and giving place to a change in the diffusion regime. In fact, as the applied electric field
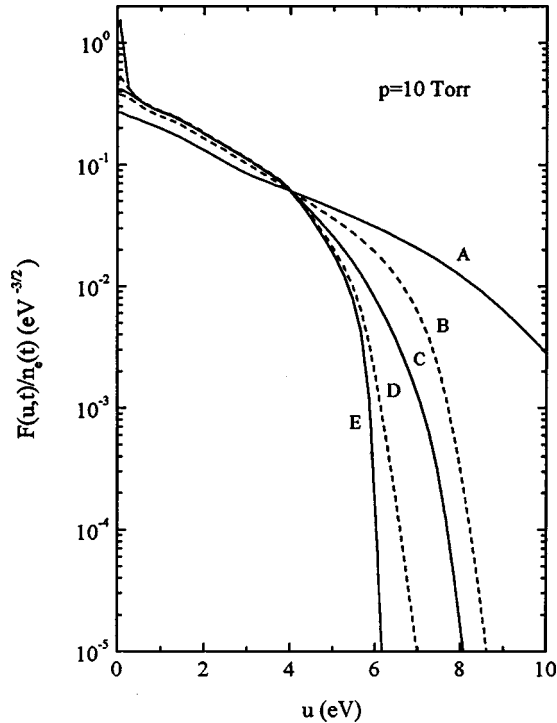
FIG. 15. EEDF calculated in the post-discharge of an $\omega/(2\pi)$ $=2.45$ GHz microwave discharge in N_2, with $p=10$ Torr and $n_e(0)=5\times10^{11}$ cm^{-3}, for the following instants in the afterglow: (A) $t=0$, (B) 10^{-7} s, (C) 10^{-5} s, (D) 10^{-4} s, and (E) 1.4×10^{-3} s.

FIG. 16. Temporal evolution of the electron rate coefficients for excitation of $N_2(A)$, $N_2(B)$, and $N_2(C)$ states (curves $A-C$), calculated in a N_2 afterglow for the same conditions as in Fig. 15. The symbols represent the rate coefficients in the discharge ($t=0$).

drops to zero at the end of the discharge, the electron density remains practically unchanged within a relatively long time interval, which originates that the radial space-charge field is maintained. This latter may vary only within the time scale for n_e variations.

With the exception of an experimental work in which an effective diffusion coefficient assuring a transition from ambipolar to free diffusion limits was derived from breakdown time delay data [21], and whose results are qualitatively in agreement with the present study, other works on the electron kinetics in a nitrogen afterglow were mainly concerned with the coupling between the EEDF and the VDF of $N_2(X,v)$ molecules [12,18], or with the coupling between the EEDF and the populations of excited electronic states [13,14]. However, Refs. [12–14] assumed the mechanism for electron losses in the afterglow to be gas-phase recombination only, while in Ref. [18] only processes that keep the electron density constant were considered.

The worthwhile conclusion to be stressed from the present paper is that although the EEDF is largely modified in the post-discharge after relatively short times as small as $\sim10^{-7}$ s, the electron density remains practically unchanged up to $t\sim10^{-5}$ s. Then $n_e(t)$ is reduced in the time interval

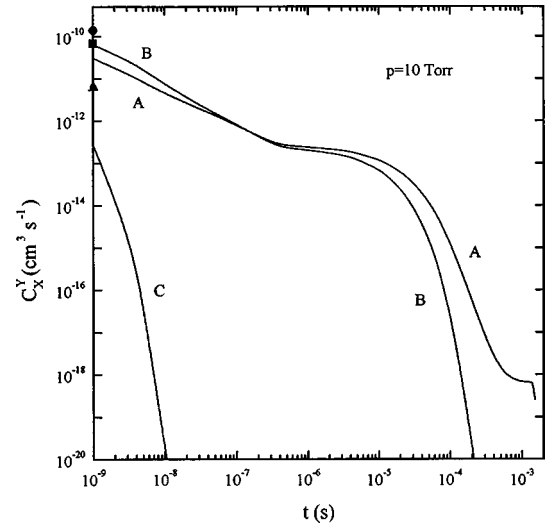$10^{-5}-10^{-4}$ s at $p=2$ Torr and $10^{-5}-10^{-3}$ s in the case of the higher value of pressure $p=10$ Torr. This behavior essentially results from the large characteristic times for electron losses by ambipolar diffusion $\sim(D_a/\Lambda^2)^{-1}$. A second important conclusion derived from the present study is that certain processes due to electron impact play a nonvanishing role in the post-discharge. This is the case for processes leading to vibrational excitation of $N_2(X,v)$ levels, as well as of stepwise excitation of $N_2(B)$ and $N_2(C)$ states from $N_2(A)$ metastables.

Work is in progress to couple the present time-dependent Boltzmann analysis to a self-consistent determination of the concentrations of $N_2(X,v)$ molecules and electronically excited states of N_2, in order that the effects of electron-superelastic collisions may be updated during the time evolution. In fact, our previous studies [9] showed that the VDF in a N_2 post-discharge begins to be modified at $t\sim10^{-4}$ s, so that the calculated data at the upper limit of the time-interval considered in this paper are merely indicative. Finally, a second weakness of the present study is associated with the neglect in the model of secondary electron production in the post-discharge, as a result of collisions between $N_2(A)$ $+N_2(a')$ or $N_2(a')+N_2(a')$ states [30], as well as of ionization processes involving vibrationally excited $N_2(X,v)$ molecules [39].

ACKNOWLEDGMENT

[1] A. Ricard, J. E. Oseguera-Pena, L. Falk, H. Michel, and M. Gantois, IEEE Trans. Plasma Sci. **18**, 940 (1990).

[2] H. Malvos, H. Michel, and A. Ricard, J. Phys. D **27**, 1328 (1994).

[3] S. Bockel, T. Belmonte, H. Michel, and D. Ablitzer, Surf. Coat. Technol. **97**, 618 (1997).

[4] C. Boisse-Laporte, C. Chave-Normand, and J. Marec, Plasma Sources Sci. Technol. **6**, 70 (1997).

[5] A. R. De Souza, M. Digiacomo, J. L. R. Muzart, J. Nahorny, and A. Ricard, Eur. Phys. J. A **5**, 185 (1999).

[6] P. Supiot, O. Dessaux, and P. Goudmand, J. Phys. D **28**, 1826 (1995).

[7] D. Blois, P. Supiot, M. Barj, A. Chapput, C. Foissac, O. Dessaux, and P. Goudmand, J. Phys. D **31**, 2521 (1998).

[8] C. Foissac, A. Campargue, A. Kachanov, P. Supiot, G. Weirauch, and N. Sadeghi, J. Phys. D **33**, 2434 (2000).

[9] P. A. Sá, and J. Loureiro, J. Phys. D **30**, 2320 (1997).

[10] N. A. Gorbunov, N. B. Kolokolov, and A. A. Kudryavtsev, Zh. Tekh. Fiz. **58**, 1817 (1988) [Sov. Phys. Tech. Phys. **33**, 1104 (1988)].

[11] J. F. Loiseau, P. Pignolet, and B. Held, J. Phys. D **25**, 745 (1992).

[12] C. Gorse, M. Capitelli, and A. Ricard, J. Chem. Phys. **82**, 1900 (1985).

[13] C. Gorse, and M. Capitelli, J. Appl. Phys. **62**, 4072 (1987).

[14] C. Gorse, M. Cacciatore, M. Capitelli, S. De Benedictis, and G. Dilecce, Chem. Phys. **119**, 63 (1988).

[15] A. A. Kudryavtsev and A. I. Ledyankin, Phys. Scr. **53**, 597 (1996).

[16] L. S. Bogdan, S. M. Levitskii, and E. V. Martysh, Zh. Tekh. Phys. **63**, 203 (1993) [Tech. Phys. **38**, 532 (1993)].

[17] S. I. Gritsinin, I. A. Kossyi, V. P. Silakov, and N. M. Tarasova, J. Phys. D **29**, 1032 (1996).

[18] N. A. Dyatko, I. V. Kochetov, and A. P. Napartovich, J. Phys. D **26**, 418 (1993).

[19] M. Capitelli, C. Gorse, and A. Ricard, J. Phys. (France) Lett. **44**, L-251 (1983).

[20] J. Borysow, and A. V. Phelps, Phys. Rev. E **50**, 1399 (1994).

[21] V. Lj. Marković, Z. Lj. Petrović, and M. M. Pejović, Plasma Sources Sci. Technol. **6**, 240 (1997).

[22] S. De Benedictis, and G. Dilecce, Chem. Phys. **192**, 149 (1995).

[23] W. P. Allis, in *Handbuch der Physik*, edited by S. Flügge (Springer, Berlin, 1956), Vol. 21, p. 383.

[24] S. C. Brown, in *Handbuch der Physik* (Ref. [23]), Vol. 22, p. 531.

[25] J. Loureiro, Phys. Rev. E **47**, 1262 (1993).

[26] L. C. Pitchford and A. V. Phelps, Phys. Rev. A **25**, 540 (1982).

[27] C. M. Ferreira and M. Moissan, Phys. Scr. **38**, 382 (1988).

[28] P. A. Sá, J. Loureiro, and C. M. Ferreira, J. Phys. D **25**, 960 (1992).

[29] L. S. Frost, and A. V. Phelps, Phys. Rev. **127**, 1621 (1962).

[30] V. Guerra and J. Loureiro, Plasma Sources Sci. Technol. **6**, 361 (1997).

[31] V. Guerra and J. Loureiro, Plasma Sources Sci. Technol. **8**, 110 (1999).

[32] S. K. Dhali and L. H. Low, J. Appl. Phys. **64**, 2917 (1988).

[33] P. M. Mul and J. Wm. McGowan, J. Phys. B **12**, 1591 (1979).

[34] S. D. Rockwood, Phys. Rev. A **8**, 2348 (1973).

[35] See, e.g., by W. H. Press, B. P. Flannery, S. A. Teukolsky, and W. T. Vetterling, *Numerical Recipes: The Art of Scientific Computing* (Cambridge University Press, New York, 1986); by L. Fox and D. F. Mayers, *Computing Methods for Scientists and Engineers* (Clarendon, Oxford, 1968).

[36] J. Bacri and A. Medani, Physica B&C **112**, 101 (1982).

[37] G. Cartry, L. Magne, and G. Cernogora, J. Phys. D **32**, 1894 (1999).

[38] J. Wm. McGowan, P. M. Mul, V. S. D'Angelo, J. B. A. Mitchell, P. Defrance, and H. R. Froelich, Phys. Rev. Lett. **42**, 373 (1979).

[39] L. G. Bol'shakova, Yu. B. Golubovskii, V. M. Telezhko, and D. G. Stoyanov, Zh. Tekh. Fiz. **60**, 53 (1990) [Sov. Phys. Tech. Phys. **35**, 665 (1990)].